

Analysing QBER and secure key rate under various losses for satellite based free space QKD

Muskan*, Ramniwas Meena†, Subhashish Banerjee‡

Department of Physics, Indian Institute of Technology, Jodhpur, India-342030

August 2023

Abstract

Quantum Key Distribution is a key distribution method that uses the qubits to safely distribute one-time use encryption keys between two or more authorised participants in a way that ensures the identification of any eavesdropper. In this paper, we have done a comparison between the BB84 and B92 protocols and BBM92 and E91 entanglement based protocols for satellite based uplink and downlink in low Earth orbit. The expressions for the quantum bit error rate and the keyrate are given for all four protocols. The results indicate that, when compared to the B92 protocol, the BB84 protocol guarantees the distribution of a higher secure keyrate for a specific distance. Similarly, it is observed that BBM92 ensures higher keyrate in comparison with E91 protocol.

Keywords— Quantum cryptography, Quantum communication, Free space communication

1 Introduction

The most developed use of quantum communication is quantum cryptography [1–5] which offers a completely secure coding mechanism. In order to provide secure quantum optical communication, quantum key distribution (QKD) uses the qubits to safely distribute one-time use encryption keys between two or more authorised participants in a way that ensures the identification of any eavesdropper. Heisenberg’s uncertainty principle and the quantum no-cloning principle provide assurance for QKD security [6, 7]. Essentially, a solution to the key distribution problem is devised by leveraging these physical characteristics of the information carrier to prevent eavesdropping. Any information obtained by an illegitimate third party about the exchanged key leads to a corresponding increase in the quantum bit error rate (QBER) of the transmitted data.

The concept of QKD was initially proposed in [8]. In [9], the first implementation of free space QKD over a 30 cm optical link was demonstrated. Since then, significant research efforts have been dedicated to developing this technology for future optical communication systems that support secure transmission of critical information. While early experimental setups were capable of sending quantum signals over distances of up to 100 km [10] using optical fiber links, the propagation limitations of optical fibers restricted QKD over fibers to only a few hundred kilometers [11]. However, using free space links offers the potential to extend these distances further [12, 13]. Free space links leverage low absorption in specific wavelength ranges

*E-mail: muskan.1@iitj.ac.in

†E-mail: meena.21@iitj.ac.in

‡E-mail: subhashish@iitj.ac.in

and non-birefringent characteristics, ensuring the preservation of polarization. To fully harness the advantages of free space communication, satellites are ideal [14]. By utilizing satellites in Earth satellite links, the path within the atmosphere can be reduced to approximately 30 km (depending on satellite elevation). Establishing a network of satellites would enable a physically secure global communication network, thereby significantly expanding the range of QKD capabilities.

In the construction of a worldwide network, satellite-based quantum communication is crucial and effective [15–23]. Free space optical (FSO) communications are the focus of these satellite-based quantum communication [24]. Free space QKD under atmospheric turbulence must be taken into account for the successful implementation of satellite-based quantum communication [25], [26], [27], [28]. For earth-to-space quantum communication to be possible, the connection attenuation must be less than 60 dB; quantum communication is not practical above this number. The following situations between Earth and space have the following link distances (L): Ground-LEO and LEO-ground link distances are 500-1400 km, ground-GEO and GEO-ground link distances are above 360,000 km, and the LEO-LEO (intersatellite link) link distance is 2000 km. LEO-GEO link distance is 35,500 km, and the GEO-GEO link distance is 40,000 km. Ground-MEO and MEO-ground link distances are 10000-30000 km, LEO-MEO link distance is 14000 km, MEO-MEO (intersatellite link distance) is also around 14000 km and MEO-GEO link distance is around 15000 to 28000 km. [29]. Quantum communication still requires additional research to address problems with security, data rate, and communication distance despite the huge success of QKD’s commercial applications in terms of scientific advancement [24, 30–33].

The process of generating a secret key using QKD involves five essential steps: authentication [34, 35], single photon transmissions, sifting, error correction, and privacy amplification [36]. Initially, a randomly generated raw key is transmitted over the quantum channel to create secret key information. Following this, the key information is exchanged over a public channel, resulting in the acquisition of the sifted key. Subsequently, error correction and privacy amplification steps are employed. The purpose of the error correction step is twofold: it corrects any errors in the received information bits and provides an estimation of the error rate. On the other hand, privacy amplification is implemented to distill a shorter yet significantly more secure final key as desired.

When assessing the effectiveness of different QKD systems, two important criteria are considered: the ‘QBER’ and the ‘keyrate’. The QBER serves as an indicator of security and is crucial for evaluating the performance of the link after error correction. If an unauthorized third party gains any knowledge about the exchanged key, it leads to an increase in the QBER. A higher QBER means that the eavesdropper can gather more information about the transmitted key, compromising the security of the legitimate recipient. It is important to note that higher QBER values in QKD systems can lower the keyrate during the error correction stage of the protocol. Therefore, it is desirable to have a low QBER and a higher keyrate in order to ensure effective and secure communication. These are the parameters on which we have performed the comparison between well known protocols BB84 and B92, along with entangled-based protocols BBM92 and E91. We have calculated the QBER and keyrate for both the uplink and downlink scenarios, considering different types of losses.

The paper is structured as follows: Sec.2 provides a concise analysis of the BB84, B92, BBM92, and E91 protocols. In Sec.3, we review different types of losses and their impact on the QBER for various protocols. Next, in Sec.4, we introduce and analyze the QBER for different protocols. Sec.5 focuses on the keyrate calculations for different protocols and examines blinding attacks specifically targeting entangled-based protocols. In Sec.6, we present numerical results and have discussions. The paper concludes with a summary of the key points.

2 QKD Protocols

QKD protocols are the foundation of secure communication enabled by quantum mechanics. These protocols establish a shared secret key between two parties, typically referred to as Alice and Bob, while ensuring that

any eavesdropping attempts are detectable. Several QKD protocols have been developed, each with its unique approach to key generation and security guarantees. Here we briefly discuss the QKD protocols used in this work:

2.1 BB84

The BB84 protocol is a QKD protocol, proposed in [8]. Its purpose is to enable two parties, traditionally named Alice and Bob, to securely generate and share a secret cryptographic key that can be used for subsequent communication. The protocol works by encoding information in quantum states, typically using photons as the carrier of information. Alice sends a sequence of photons to Bob, with each photon randomly prepared in one of four possible states, which are represented by two different orthogonal polarizations (e.g., horizontal/vertical or diagonal/anti-diagonal). Bob receives the photons and measures their polarization using a randomly chosen basis, either horizontal/vertical or diagonal/anti-diagonal. Due to the uncertainty principle of quantum mechanics, any attempt to eavesdrop on the communication would unavoidably introduce errors in the polarization measurements, allowing Alice and Bob to detect the presence of an eavesdropper. After the transmission is complete, Alice and Bob compare a subset of their measurement results to check for errors and potential eavesdropping. They discard any bits that have errors, and the remaining bits form a shared secret key that can be used for subsequent communication, such as encrypting and decrypting messages.

2.2 B92

The B92 protocol is another QKD protocol [37]. The B92 protocol is a simplified version of the BB84 protocol, requiring fewer quantum states to transmit information.

Alice sends a sequence of photons to Bob, with each photon randomly prepared in one of two possible states, represented by two different orthogonal polarizations. Bob randomly chooses to measure the photons in either the horizontal/vertical or diagonal/anti-diagonal basis. If Bob measures a photon with the same polarization as Alice sent, he obtains a bit value of "0", while if he measures a photon with the orthogonal polarization, he obtains a bit value of "1". If Bob measures a photon with the same polarization as Alice sent, but with a different intensity, he does not obtain any bit value. After the transmission is complete, Alice and Bob publicly disclose the basis used for each photon transmission. Alice and Bob compare a subset of their measurement results to check for errors and potential eavesdropping. They discard any bits that have errors, and the remaining bits form a shared secret key that can be used for subsequent communication. The B92 protocol is simpler and faster than the BB84 protocol, but it is less secure, as an eavesdropper can obtain information by manipulating the photon intensity without being detected. Despite this limitation, the B92 protocol remains an important contribution to the field of quantum cryptography, as it illustrates the potential for quantum information processing with a minimal set of resources.

2.3 E91

The E91 is a QKD protocol that is based on the idea of entanglement and is developed in [38]. The procedure operates as follows:

There is a source that distributes maximally entangled pairs of qubits to Alice and Bob, for example, states of the type

$$|\psi^-\rangle_{AB} = \frac{1}{\sqrt{2}}(|01\rangle_{AB} - |10\rangle_{AB}). \quad (1)$$

Alice and Bob measure an observable that is randomly selected from the sets $\{A_i\}$ and $\{B_i\}$, respectively, for each of these bipartite states $|\psi^-\rangle_{AB}$. Figure 1 shows these observables, which are spin components located in the Bloch sphere's x - z plane. In general, these operators are defined as

$$A_i = \cos\varphi_i^A + \sin\varphi_i^A \quad (2)$$

$$B_i = \cos\varphi_i^B + \sin\varphi_i^B \quad (3)$$

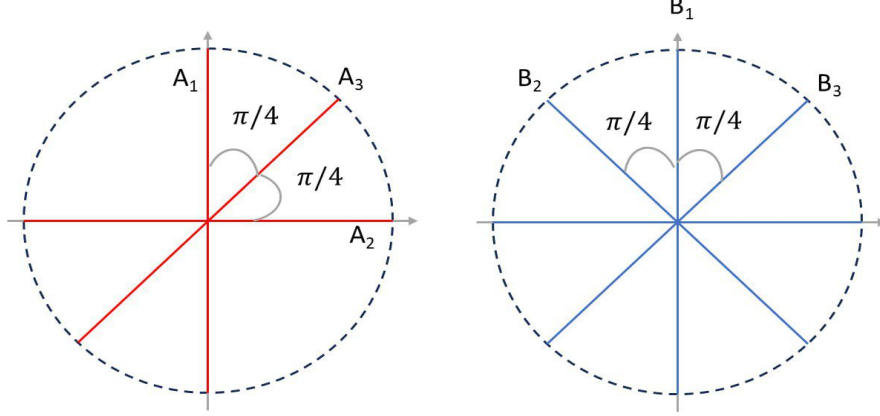


Figure 1: Measurements directions for the Ekert protocol. The measurements are depicted in the x - z plane of the Bloch sphere. On the left side are the three different measurements that Alice can choose between, and on the right side Bob's possible measurement directions are shown.

with $\varphi_1^A = 0$, $\varphi_2^A = \frac{\pi}{2}$, and $\varphi_3^A = \frac{\pi}{4}$ for Alice and $\varphi_1^B = 0$, $\varphi_2^B = \frac{-\pi}{4}$, $\varphi_3^B = \frac{\pi}{4}$ for Bob. In terms of the measurement operators $Z = |0\rangle\langle 0| - |1\rangle\langle 1|$ and $X = |+\rangle\langle +| - |-\rangle\langle -|$, the measurements can also be written as

$$\begin{aligned} A_1 &= Z & B_1 &= Z \\ A_2 &= X & B_2 &= \frac{1}{\sqrt{2}}(Z - X) \\ A_3 &= \frac{1}{\sqrt{2}}(Z + X) & B_3 &= \frac{1}{\sqrt{2}}(Z + X). \end{aligned} \quad (4)$$

The measurements of Alice and Bob, A_1 and B_1 as well as A_3 and B_3 , are taken in the same direction.

The next stage is for Alice and Bob to reveal the measurement directions they decided upon. The pairs (A_1, B_1) and (A_3, B_3) are examples of those where the directions match, and they produce totally anti-correlated outputs. The results of these measurements thus constitute the sifted key by inverting all bits for one side. To determine how much knowledge an eavesdropper knows about the key, the results from the measurement pairs (A_1, B_3) , (A_1, B_2) , (A_2, B_3) , and (A_2, B_2) are employed. This is accomplished by examining a supposedly CHSH inequality. The CHSH inequality is a limit on the expectation values of some classical correlations. It is a component of a wider collection of inequalities known as Bell inequalities. Assume you have the four standard random variables A_1 , A_2 , B_2 , and B_3 . Assume that each of them can take either $+1$ or -1 as its value. It is simple to confirm that $A_1(B_3 + B_2) + A_2(B_3 - B_2) = \pm 2$ by simply ruling out all other options. By taking the expectation value of these quantities over N assignments of the random variables, we get

$$|\langle A_1(B_3 + B_2) + A_2(B_3 - B_2) \rangle| \leq 2, \quad (5)$$

where $\langle A_i B_j \rangle = \frac{1}{N} \sum A_i^\nu B_j^\nu$, and A_i^ν and B_j^ν represent the assigned values ν to the random variables A_i and B_j . We can now consider A_1, A_2, B_2, B_3 to be quantum observables as described in the Ekert protocol. The expectation value for their products is then given by

$$\langle A_i B_j \rangle = \text{Tr}(A_i \otimes B_j \rho). \quad (6)$$

Using the measurement directions defined in the Ekert protocol, we can evaluate their expectation values with respect to the state $\rho = |\Psi^-\rangle\langle\Psi^-|$. For instance, the expectation value of A_1 and B_3 is

$$\langle A_1 B_3 \rangle = \langle \Psi^- | (Z \otimes \frac{1}{\sqrt{2}}(Z + X)) | \Psi^- \rangle = -\frac{1}{\sqrt{2}}. \quad (7)$$

In this way we can evaluate all terms in the sum of expectation values S and find that

$$S = 2\sqrt{2}. \quad (8)$$

This indicates that Alice and Bob share a maximally entangled state because it violates the CHSH inequality, derived above. A maximally entangled bipartite state cannot be entangled with a third party. Hence, Eve is unaware of the key in this situation. In actuality, this is the greatest value of S that is possible. The CHSH inequality can generally be violated even with smaller values of S . Eve might know something about the key in this situation. As long as there is some violation of the CHSH inequality, it is still possible to extract a secret key from this data. It is impossible to create a secret key, as demonstrated in [39], if $S \leq 2$, which denotes that Alice and Bob share a pair of separable states. If their measurement findings pass the test, Alice and Bob can continue with the protocol and use privacy amplification along with error correction to get the final secret key.

2.4 BBM92

BBM92 is another entangled based protocol. The protocol was first proposed in 1992[40]. The protocol makes use of pairs of entangled particles, known as EPR pairs, which are distributed between Alice and Bob. Here's how the BBM92 protocol works: Alice creates a set of EPR pairs and sends one particle from each pair to Bob. Bob randomly measures each incoming particle using one of two bases: the standard basis (Z-basis) or the Hadamard basis (X-basis). Alice tells Bob which basis she used to prepare each particle. Bob discards all the measurements that were made in the wrong basis, and keeps the rest. Alice and Bob publicly compare a subset of their remaining measurements to estimate the error rate. Alice and Bob use the remaining measurements to generate a secret key by applying a reconciliation procedure and a privacy amplification procedure. Alice and Bob can now use their secret key for secure communication. The BBM92 protocol is secure against eavesdropping because any attempt to measure the particles in transit will disturb the entanglement and be detected by Alice and Bob. Additionally, the use of entangled pairs ensures that any attempt to clone the particles will also be detected.

3 Different type of losses

In QKD, various types of losses can occur during the transmission and processing of quantum information. These losses can have an impact on the performance and security of the QKD system. We describe here various losses like geometrical loss, optical loss, and atmospheric losses including turbulence loss and scattering loss. These losses are considered when calculating the QBER and key rate. These losses are factored into the evaluation to determine their influence on the system's performance and security.

3.1 Geometrical loss

Geometrical loss is a measure of the reduction in signal power as it propagates from a transmitter to a receiver. It is determined by the ratio of the surface area of the receiver aperture to the surface area of the transmitter beam at the receiver [41, 42]. The surface area of the transmitter beam is affected by its divergence, which causes it to spread out as it travels through space. Therefore, geometrical loss is primarily influenced by the divergence of the beam and the distance between the transmitter and receiver. The geometrical loss can be determined by the formula stated as:

$$\text{Geometrical loss} = 10 \log \left[\frac{d_r^2}{(d_t + (L\theta))^2} \right], \quad (9)$$

here d_r represents diameter of the receiver (in m), d_t represents diameter of the transmitter (in m), θ is divergence angle of the beam (in mrad), L is the distance between transmitter and receiver.

3.2 Turbulence Loss-Induced Scintillation loss for Uplink and Downlink

Scintillations are characterized by sudden and rapid changes in the phase and amplitude of a wave. These fluctuations occur due to the local and rapid variations in the refractive index of the medium through which the wave is traveling. When laser radiation propagates through a turbulent medium, it experiences both temporal and spatial fluctuations in irradiance, which are referred to as scintillation or atmospheric turbulence-induced irradiance fluctuations [43]. This phenomenon is a consequence of the random and irregular changes in the refractive index of the atmosphere that the laser beam encounters during propagation. The scintillation index is the most commonly used measure to quantify the magnitude of scintillation

$$\sigma_I^2 = \frac{\langle I^2 \rangle - \langle I \rangle^2}{\langle I \rangle^2} = \frac{\langle I^2 \rangle}{\langle I \rangle^2} - 1, \quad (10)$$

where I signifies the optical wave's irradiance and $\langle \rangle$ stands for the ensemble average, which is equivalent to the long-time average if the process is assumed to be ergodic. The scintillation index in weak fluctuation theory is proportional to the Rytov variance given by:

$$\sigma_1^2 = 1.23 C_n^2 k^{7/6} L^{11/6}, \quad (11)$$

where turbulence strength is measured by C_n^2 , $k = \frac{2\pi}{\lambda}$, is the optical wave number and L is the path length between the communication transmitter and receiver. The value of C_n^2 is assumed to remain constant for horizontal paths up to a few kilometres, whereas for downlink (space-to-ground) or uplink (ground-to-space) of altitude h has to be use. For vertical or slant path, the so-called Hufnagel-Vallyely model is generally regarded as representative of continental conditions [44].

3.2.1 Hufnagel-Valley Model

$$C_n^2(h) = 0.00594 \left(\frac{v}{27} \right)^2 (10^{-5}h)^{10} \exp \left(-\frac{h}{1000} \right) + 2.7 \times 10^{-16} \exp \left(-\frac{h}{1500} \right) + A \exp \left(-\frac{h}{100} \right), \quad (12)$$

where $A = C_n^2(0)$ is the ground-level of C_n^2 and v is the rms wind speed. For our numerical calculations, we have assumed $v = 21 \text{ m/s}$ and $A = 1.7 \times 10^{-14}$ for the $C_n^2(h)$ model. Scintillation loss of the transmission system (in dB) is given by [45]:

$$a_{sci} = [3.3 - 5.77(-\ln p_{thr})^{\frac{1}{2}}] (\sigma_I^2(D))^{0.4}, \quad (13)$$

Here p_{thr} is the probability that the receiver power falls below the limit. $\sigma_I^2(D)$ is the aperture-averaged scintillation index. This is the factor which includes the concept of uplink and downlink.

When it comes to the downlink of space-to-ground communications, the beam experiences distortion upon entering the Earth's atmosphere. The scintillation near the center of the received wave at ground level can be effectively represented and modeled as a plane wave [46].

For downlink, the aperture averaged scintillation index for plane wave is given by:

$$\sigma_I^2(D) = \exp \left[\frac{0.49\sigma_1^2}{\left(1 + 0.65d^2 + 1.11\sigma_1^{12/5} \right)^{7/6}} + \frac{0.51\sigma_1^2(1 + 0.69\sigma_1^{12/5})^{-5/6}}{1 + 0.90d^2 + 0.62d^2\sigma_1^{12/5}} \right] - 1, \quad (14)$$

where σ_1^2 is the Rytov variance for plane wave and is given by above Eq.(11). Also,

$$d = \sqrt{\frac{K d_r^2}{4L}}, \quad (15)$$

where d_r is the receiver aperture size and K is the wave number. Further, L represents the distance between the transmitter and receiver in a communication system.

For an uplink, where the atmospheric turbulence begins just outside the transmitting aperture, we can assume a spherical wave and the expression for the apertured average scintillation index for spherical wave is given by:

$$\sigma_I^2(D) = \exp \left[\frac{0.49\sigma_2^2}{\left(1 + 0.18d^2 + 0.56\sigma_2^{12/5}\right)^{7/6}} + \frac{0.51\sigma_2^2(1 + 0.69\sigma_2^{12/5})^{-5/6}}{1 + 0.90d^2 + 0.62d^2\sigma_2^{12/5}} \right] - 1, \quad (16)$$

where σ_2^2 is the Rytov variance for spherical wave and is given by:

$$\sigma_2^2 = 0.4\sigma_1^2. \quad (17)$$

3.2.2 Turbulence-Induced Beam Wandering Effect

In the context of the uplink scenario for FSO from the ground to a satellite, the transmitter is located close to the Earth's atmosphere, while the receiver is positioned in the far field. In this configuration, the size of the transmitter beam is typically smaller than the outer scale of turbulence, known as L_0 . Consequently, the instantaneous point of maximum irradiance, often referred to as the "hot spot," will be displaced from its original on-axis position. As a result, this displacement of the "hot spot" due to the beam size being smaller than the eddies' size can cause a pointing error, leading to the misalignment of the beam and missing the intended target. When the eddies' size is smaller than the beam size, only a small fraction of the beam will undergo diffraction and scattering independently.

In Ground-to-Satellite FSO communication, the laser beam encounters random inhomogeneities in the atmosphere caused by fluctuations in the refractive index. These fluctuations are quantified by the refractive index structure parameter, denoted as $C_n^2(h)$, which characterizes the strength of turbulence in the atmosphere at different heights above the ground. Obtaining accurate measurements of $C_n^2(h)$ is crucial and can be achieved by measuring parameters such as temperature (T), pressure (P), wind speed (V), and spatial fluctuations in temperature (ΔT) along the propagation path [47]:

$$C_n^2 = \left[79 \times 10^{-6} \frac{P}{T^2} \right] C_T^2, \quad (18)$$

here C_T^2 is the temperature structure parameter which is determined by taking the measurements of mean square temperature between two points separated by certain distance along the propagation path (in $\text{deg}^2/\text{m}^{-2/3}$) and is expressed as:

$$C_T^2 = \langle \Delta T^2 \rangle r^{-1/3}, \quad (19)$$

where $\Delta T = T_1 - T_2$ (T_1 and T_2 are the temperatures of two arbitrary points separated by a distance r) and the angle bracket $\langle \rangle$ denotes an ensemble average. The Profile model of the refractive index structure parameter ($C_n^2(h)$) describes how it varies with altitude (h). Turbulence in the atmosphere gives rise to the formation of eddies with different refractive indices and sizes. In the FSO uplink scenario, when the beam size is smaller than the outer scale of turbulence (L_0), the entire beam undergoes random deflection from its original path. This phenomenon, known as beam wander, results in a significant change in the direction of the beam. The statistical characterization of the beam wander effect is represented by the variance of beam wander displacement ($\langle r_c^2 \rangle$) and can be expressed as: [48]

$$\langle r_c^2 \rangle = 0.54(H - h_0)^2 \sec^2(\theta) \left(\frac{\lambda}{2W_0} \right)^2 \left(\frac{2W_0}{r_0} \right)^{5/3}, \quad (20)$$

where θ is the zenith angle, λ is the operating wavelength, W_0 is the transmitter beam radius, H and h_0 are the altitude of satellite and transmitter respectively. For ground based transmitter, $h_0 = 0$ and satellite

altitude $H = h_0 + L(\cos(\theta))$ where L is propagation length. The other parameter r_0 is the atmospheric coherence length (or Fried parameter) defined by:

$$r_0 = \left[0.423 K^2 \sec(\theta) \int_{h_0}^H C_n^2(h) dh \right]^{-3/5}, \quad (21)$$

where K is the optical wave number.

The beam wander effect will lead to effective pointing error of the beam σ_{Pe} given as [48]

$$\sigma_{Pe}^2 = \langle r_c^2 \rangle = \left[1 - \left(\frac{C_r^2 W_0^2 / r_0^2}{1 + C_r^2 W_0^2 / r_0^2} \right)^{1/6} \right]. \quad (22)$$

In the above equation, the parameter C_r is a scaling constant typically in the range from 1 to 2π . The pointing error induced by beam wander contributes to an increase in the scintillation index, which differs from the prediction of conventional Rytov theory [49]. In the first-order Rytov theory, the scintillation index, denoted as σ_I^2 , is expressed as the sum of longitudinal $\sigma_{I,l}^2$ and radial $\sigma_{I,r}^2(r, l)$ components. However, when accounting for the beam wander effect in FSO uplink scenarios, the increase in $\sigma_{I,l}^2(L)$ should be considered. This is because the effect of beam wander can cause slight flattening of the beam and an increase in the long-term beam profile near the bore-sight.

The Scintillation produced by beam wander effect is expressed as:

$$\sigma_{I,l}^2(L) = 5.95(H - h_0)^2 \sec^2(\theta) \left(\frac{2W_0}{r_0} \right)^{5/3} \left(\frac{\alpha_{Pe}}{W} \right)^2. \quad (23)$$

In the above equation, $\alpha_{Pe} = \sigma_{Pe}/L$ is the angular pointing error due to beam wander effect.

3.3 Scattering loss

The primary factors contributing to loss in the atmospheric channel are absorption and scattering processes [50]. Absorption in the atmosphere occurs when the photons of the beam interact with dispersed particles such as water vapors, dust, ice, and organic molecules. However, it's important to note that atmospheric absorption is dependent on the wavelength of the beam. To minimize absorption effects, the wavelength range of FSO communication systems is carefully selected to ensure minimal absorption.

Scattering refers to the phenomenon where a beam of radiation is dispersed into various directions due to physical interactions.

Rayleigh scattering occurs when molecules and atmospheric gases scatter light with sizes significantly smaller than the wavelength of the incident light. Mie scattering occurs when the diameter of particles is equal to or larger than one-tenth of the wavelength of the incident laser beam. In the context of FSO at terrestrial altitudes, Mie scattering is the primary cause of attenuation at the laser wavelengths used. Fog and haze droplets, which dominate the Mie-scattering effect, are responsible for the significant attenuation of transmitted optical beams in free space. Non-selective scattering refers to the scattering phenomenon caused by rainfall, where the radius of raindrops is considerably larger than the wavelength of typical FSO systems. Due to this size difference, the laser beam is capable of passing through raindrops or particles with minimal scattering effects. Hence attenuation is mainly due to Mie-scattering.

The measurement of atmospheric visibility provides a valuable indication of the prevailing environmental conditions in the atmosphere. Visibility is the distance that a parallel luminous beam can travel through the atmosphere until its intensity decreases by 2% of its original value. This measurement is conducted using a wavelength of 550 nm, which corresponds to the wavelength that the human eye is most sensitive to.

Mie scattering theory can be utilized to predict the attenuation caused by fog. The specific attenuation of fog given by common empirical model for Mie scattering -

$$\beta_{fog}(\lambda) = \frac{3.91}{V} \left(\frac{\lambda}{550} \right)^{-P}, \quad (24)$$

Where $V(\text{km})$ stands for visibility range, $\lambda(\text{nm})$ is the operating wavelength and P is the size distribution coefficient of scattering. According to Kruse Model [51]

$$P = \begin{cases} 1.6 & V > 50\text{km} \\ 1.3 & 6\text{km} < V < 50\text{km} \\ 0.585V^{1/3} & V < 6\text{km} \end{cases}. \quad (25)$$

The formula mentioned above for specific attenuation of fog does not account for dense fog conditions. Recent investigations have revealed that wavelength dependency is absent when visibility decreases below 500m. As a result, the parameter "P" in the Kim formula [51] has been adjusted accordingly to accommodate these findings. The modified formula is as follows:

$$P = \begin{cases} 1.6 & V > 50\text{km} \\ 1.3 & 6\text{km} < V < 50\text{km} \\ 0.16V + 0.34 & 1\text{km} < V < 6\text{km} \\ V - 0.5 & 0.5\text{km} < V < 1\text{km} \\ 0 & V < 0.5\text{km} \end{cases}. \quad (26)$$

As $T_a = \exp(-\sigma L)$.

In terms of scattering coefficient above equation can be written as:-

$$T_a = \exp(-\beta_{fog} L). \quad (27)$$

3.4 Optical loss

The optical losses in FSO systems are primarily attributed to imperfections in the optical elements utilized at the transmitter (η_t) and receiver (η_r). The losses are expressed in decibels (dB) and can be calculated using the formula described in the [52]

$$L_{opt} = 10\log(\eta_t \eta_r). \quad (28)$$

4 QBER

The QBER is a measure of the ratio of incorrect bit counts to the total number of received bit counts. It is used to quantify the probability of obtaining a false detection in comparison to the total probability of detection per pulse. The QBER is influenced by two main components: the signal component and the dark count component. It is assumed that the channel is an exponentially decaying function of distance. Thus, channel transmission T_{chan} can be written as

$$T_{chan} = 10^{-\sigma \cdot L/10}, \quad (29)$$

where σ is loss coefficient. It includes all types of above calculated losses.

4.1 QBER for BB84

In BB84 protocol, the QBER can be calculated as [53]:

$$e_{84} = p_{pol} + \frac{p_{dark}}{\mu \cdot T_{chan} \cdot \eta_{det} \cdot 2}, \quad (30)$$

where p_{pol} is the probability of a photon arriving at the wrong detector, leading to false identification of polarization and is given by $p_{pol} = \frac{1-V_f}{2}$ where V_f is fringe visibility, p_{dark} is the probability of a dark count registered in a detector, T_{chan} is the transmittance of the free space channel, μ is the mean photon number of the signal, and η_{det} is the quantum efficiency of the detector.

4.2 QBER for B92

The B92 protocol utilizes basis states to determine the code values. This results in 50% of cases using the same basis for coding and decoding, and 50% detecting differences in used bases. The number of usable bits equals 25% of the total received bits. The QBER parameters for the B92 protocol are as follows [53]:

$$e_{92} = p_{pol} + \frac{p_{dark}}{\mu \cdot T_{chan} \cdot \eta_{det}}. \quad (31)$$

Here p_{dark} is the probability of dark count, μ is the average number of photons in a pulse, T_{chan} is the transmittance of the channel, η_{det} is the quantum efficiency of the detector and p_{pol} is the probability of a photon arriving at the wrong detector and $p_{pol} = \frac{1-V_f}{2}$.

4.3 QBER for BBM92

The QBER for BBM92 depends on various factors such as the properties of the quantum channel, the quality of the detectors used, and the presence of any eavesdroppers. In the assumed model, the channel is characterized as an exponential decay function with respect to distance. As a result, the transmission of the channel, denoted as T_{chan} , can be expressed as follows

$$T_{chan} = 10^{-\sigma \cdot L/10}, \quad (32)$$

where σ is loss coefficient. In one beam splitter with transmission, we combine all losses to each receiver from the channel, detectors, and optics.

$$\alpha_L = \eta_{det} \cdot T_{chan}(L). \quad (33)$$

The parameter η_{det} represents the cumulative effect of distance-independent losses within the system. The coincidence probability is divided into two components: p_{true} , which denotes the probability of a genuine coincidence between a pair of entangled photons and p_{false} , which represents the probability of a false coincidence. In an ideal source, false coincidences can only arise from a combination of a photon and a dark count or two dark counts [11]. When dual fire events are insignificant, the following expression holds in the limit:-

$$p_{coin} = p_{true} + p_{false}. \quad (34)$$

We must choose a location for the source. Setting the source at a distance of $L - x$ from Bob and x from Alice, we get

$$p_{true} = \alpha_x \alpha_{L-x} = \eta_{det} \alpha_L, \quad (35)$$

$$p_{false} = 4\alpha_x d + 4\alpha_{L-x} d + 16d^2. \quad (36)$$

Keeping only terms which are second order in α_x and d , it can be observed that the probability of a true coincidence remains constant with respect to x , while the false coincidence rate changes. By performing a straightforward optimization, it can be determined that the false coincidence rate reaches its minimum value at a distance halfway between Alice and Bob. The value of this minimum false coincidence rate can be calculated using the given formula:

$$p_{false} = 8\alpha_{L/2} d + 16d^2. \quad (37)$$

The QBER is given by

$$e_{M92} = \frac{p_{false}/2 + p_{true}}{p_{coin}}. \quad (38)$$

4.4 QBER for E91

QBER for $E91$ is given by [11]

$$e_{91} = \frac{p_{false}/3 + b p_{true}}{p_{coin}} \text{label}e91. \quad (39)$$

where $\frac{1}{3}$ factor is used because in $E91$ we use three bases, while in $BBM92$ we use two therefore the $\frac{1}{2}$ factor in Eq.(38).

5 Keyrate

Key rate, in the context of QKD, refers to the rate at which a secure cryptographic key can be generated and shared between two communicating parties, typically referred to as Alice and Bob. It quantifies the speed or efficiency at which error-free key bits can be securely exchanged and determines the practicality and effectiveness of a QKD system. The key rate is measured in bits per second (bps) and is influenced by factors such as the quality of transmitted quantum states, detection efficiency, channel losses, and potential eavesdropping attempt. The key rate serves as a benchmark for evaluating the effectiveness and practicality of protocols using QKD. In the calculation of key rate, the QBER is considered, which includes all types of losses discussed earlier. The QBER, denoted by e , incorporates the effects of various losses, including geometrical loss, optical loss, atmospheric losses like turbulence loss and scattering loss, and other factors that impact the security and performance of the QKD system are discussed above. By accounting for these losses in the QBER, the key rate provides a comprehensive assessment of the utility and efficiency of QKD protocols.

5.1 Keyrate for BB84

The secure key generation rate against PNS attack for the BB84 protocol is given by [54]:

$$R_{BB84} = \frac{1}{2} P_{click} (1 - \tau' + F(e_{84})h(e_{84})). \quad (40)$$

and

$$\tau' = \tau \left(\frac{e_{84}}{\beta} \right), \quad (41)$$

where β security parameter defined as $\beta = \frac{P_{click} - P'}{P_{click}}$ and

$$P' = 1 - (1 + \mu + \frac{\mu^2}{2} + \frac{1}{2} \frac{\mu^3}{6}) \exp(-\mu). \quad (42)$$

$F(e_{84})$ is error correction efficiency, τ is fraction of the key to be discarded during privacy amplification, $\tau(e_{84}) = \log(1 + 4e_{84} - 4e_{84}^2)$ if $e_{84} < 1/2$ and $\tau(e_{84}) = 1$ if $e_{84} > 1/2$, And $h(e_{84})$ is binary shannon entropy given by

$$h(e_{84}) = -e_{84} \log_2 - (1 - e_{84}) \log_2 (1 - e_{84}). \quad (43)$$

In the context of the standard BB84 protocol, an essential parameter of interest is the system's signal, which is commonly referred to as P_{click} . This quantity represents the overall anticipated probability that Bob will observe the detection of a photon during a specific pulse. Typically, P_{click} is determined by considering two distinct sources that can independently trigger a detection event. These sources encompass photons transmitted by Alice and background dark counts [55].

$$P_{click} = p_{signal} + p_{dark} - p_{signal}p_{dark}. \quad (44)$$

The probability of Bob's detector firing due to a photon emitted by Alice's source is denoted as p_{signal} . On the other hand, p_{dark} represents the probability of a dark count occurring in Bob's detector. Since each of

Bob's detectors has a specific probability of dark counts per time slot in the absence of a real signal, the cumulative contribution of dark counts to the detection event is determined by the following relationship:

$$p_{dark} = 4d. \quad (45)$$

The presence of dark counts in the detection process is primarily determined by the characteristics of the detectors. Dark counts tend to become more significant when the probability of Bob's detector firing due to a photon from Alice's source, p_{signal} is small. Dark counts can arise from various sources such as thermal fluctuations in the detector and stray counts. In the equation mentioned above, the coefficient 4 is present because there are four detectors in the passive module, indicating that the dark count is four times larger than the parameter D . In addition, the number of dark counts occurring within the measurement time window can be expressed as four times larger than D . Furthermore, the dark count per measurement time window is given by a number of dark counts per measurement window:

$$d = Dt_w. \quad (46)$$

The equation mentioned above relates the dark counts per measurement time window to the dark count rate of the detectors, represented by D , and the duration of the measurement time window, denoted as t_w . It is important to note that the expression assumes the neglect of simultaneous occurrences of signal and dark count events when both p_{signal} and p_{dark} are small.

Additionally, it is important to emphasize that QKD systems are implemented either using fiber optics or free space channels. As the channel of interest here, we consider the free space link. The atmospheric channel is susceptible to a variety of undesirable transmission phenomena, including atmospheric scattering, absorption and turbulence. These phenomena can result in photon losses during the propagation, leading to a condition known as decoherence. Decoherence poses a significant challenge in achieving successful free space QKD. Therefore, in addition to the P_{click} parameter, the total transmission efficiency becomes another important figure of interest. In the case of a free space channel with relatively high link loss, the contribution of the signal to the detection event is greatly influenced by the total transmission efficiency η_{tot} , which can be formulated as:

$$\eta_{tot} = T_{chan}\eta_{det}, \quad (47)$$

where T_{chan} is the quantum channel transmission and η_{det} is the detector efficiency. Depending on the link scenario, T_{chan} can be A_{atm}^{GS-GS} , A_{atm}^{GS-SL} , A_{atm}^{SL-SL} .

In the context of satellite-to-ground (downlink), the light signal emitted from the satellite travels through a relatively long vacuum distance before encountering the unpredictable and troublesome atmosphere. On the other hand, in the case of ground-to-satellite (uplink), the beam spreading effect caused by turbulence occurs primarily in the initial part of the path. In contrast, when it comes to satellite-to-satellite links, turbulence does not occur at all. The atmospheric losses in a point-to-point link can be given by [55]:

$$A_{atm}^{GS-GS} = \exp(-\sigma L), \quad (48)$$

where σ is used to denote the attenuation coefficient of light signal after passing through the atmosphere. The quantum channel transmission of both ground-to-satellite and satellite-to-ground links, excluding the point-to-point link, can be calculated as:

$$A_{atm}^{GS-SL} = T_{chan}^{B_\theta}. \quad (49)$$

In the Ground-to-Satellite direction, B_θ is the Zenith angle, and T_{chan} is atmospheric transmission at Zenith angle. In the scenario of a Satellite-to-Satellite link, where there is no atmosphere present, the channel attenuation is provided as:

$$A_{atm}^{SL-SL} = 1. \quad (50)$$

In general, photon sources are governed by the Poisson probability distribution. Utilizing the characteristic of laser pulses following the Poisson number distribution, the distribution of photon pulses can be mathematically represented as follows:

$$P(n, \mu) = \frac{\mu^n}{n!} \exp(-\mu). \quad (51)$$

The Poisson probability distribution, denoted as $P(n, \mu)$, characterizes the distribution of photons in each weak laser pulse emitted by the transmitter, assuming that there are n photons in a pulse. The parameter μ represents the average number of photons per weak laser pulse.

During the process of communication, the photons being transmitted encounter various disturbances and alterations in the channel. These disturbances encompass phenomena such as reflection, absorption, and scattering. In order to understand how these undesirable channel characteristics affect the transmitted photon pulses, the binomial probability distribution rule is applied. Accordingly, when photons propagate through the channel, the probability of registering at least one photon at the receiver can be expressed using the probability distribution

$$P_n \geq 1 = \sum_{k=1}^n C_n^k (1 - \eta_{tot})^{n-k} = 1 - (1 - \eta_{tot})^n. \quad (52)$$

Additionally, the quantum channel efficiency η_{Qchann} can be calculated by multiplying Eqs.(51) and (52) together. Quantum channel efficiency is given by η_{Qchann}

$$\begin{aligned} \eta_{Qchann} &= \sum_{n=1}^{\infty} P(n, \mu) P_n \geq 1, \\ &= \exp(-\mu) \sum_{n=1}^{\infty} \frac{\mu^n}{n!} [1 - (1 - \eta_{tot})^n], \\ &= 1 - \exp(1 - \eta_{tot})^n. \end{aligned} \quad (53)$$

Based on the behaviour of p_{signal} ,

$$p_{signal} = 1 - \exp(-\mu\eta_{tot}), \quad (54)$$

P_{click} diminishes with increasing distance between the remote communicating parties. In the above expression, the symbol μ represents the average number of photons per pulse. In the case of an ideal single photon source, μ is equal to 1. However, for a Poisson source, μ becomes a variable that requires optimization. The arrival of single photon signals at Bob's detector site is influenced by the overall probability of η_{tot} due to losses in the quantum channel. These single photon signals, when detected, contribute to the detection process.

5.2 Keyrate for B92

The secure key generation rate of the B92 protocol against photon number splitting attack can be formulated as [54]:

$$R_{B92} = \frac{1}{4} P_{click} \{ (1 - \tau' + F(e_{92})h(e_{92})) \}. \quad (55)$$

In B92, only 25% of the bits transmitted will be detected by Bob, i.e., only 25% of the raw key bits should be kept. Hence $\frac{1}{4}$ is the Sifting Factor. All the other expressions are defined in Sec.5.1.

5.3 Keyrate for BBM92

The keyrate for BBM92 protocol against double blinding attack is given by [11]:

$$R_{BBM92} = \frac{p_{coin}}{2} \{ \tau(e_{M92}) + f(e_{M92})(e_{M92} \log_2(e_{M92}) + (1 - e_{M92}) \log_2(1 - e_{M92})) \}, \quad (56)$$

τ is fraction of the key to be discarded during privacy amplification, $f(e_{M92})$ is error correction factor, p_{coin} is the coincidence probability which has already been explained in Sec.4.3.

5.3.1 Blinding Attacks: (Single and Double Blinding Attacks)

In the context of the BBM92 protocol, the existing blinding attack are of the intercept and resend type. In this type of attack, a malicious entity, often referred to as Eve, intercepts the signal that was originally intended for Bob. Eve then proceeds to perform measurements using random bases in order to obtain the raw key, just as Bob would have done in the intended communication process. To conceal her presence, Eve forwards a signal to Bob whenever she successfully obtains a measurement result. This signal ensures that Bob receives an identical outcome, while in the case of diagonal alignment, no detection occurs at all. In practical implementation using QKD devices [56], Eve employs techniques to blind Bob's detectors to single-photon detection. She achieves this by manipulating the detectors to shift from Geiger mode to linear mode, where a detector only registers a click if the incoming signal intensity exceeds a preset discriminator threshold, denoted as I_{th} . After each detection, Eve sends a bright pulse with linear polarization aligned to her own measurement result. When Eve and Bob randomly select identical measurement bases, the pulse deterministically generates a click in one of Bob's detectors. This ensures that Bob's measurement outcomes match those of Eve because the pulse is either fully reflected or transmitted at Bob's polarizing beamsplitter. However, to prevent double counting and incorrect results when Eve and Bob randomly select bases that are diagonal to each other, Eve adjusts the intensity of the pulses to be lower than twice the threshold intensity of the detectors. Consequently, the pulse is split in half at Bob's polarizing beamsplitter, resulting in an output that is insufficient to surpass the threshold and produce a click in either of Bob's detectors. The objective of the attack is for Eve to obtain an exact replica of Bob's key at the conclusion of the raw key distribution process. If Alice and Bob are sufficiently satisfied with the measured QBER on a subset of the key, Eve can eavesdrop on the error correction protocol that Alice and Bob employ. By performing the same operations as Bob during the error correction phase, Eve can successfully acquire an exact copy of the sifted key in the end. One limitation of single-blinding attacks is that, on average, Bob's resulting key size is reduced by half compared to what he would have obtained without the attack. This reduction occurs because approximately half of the time, the randomly chosen measurement bases of Eve and Bob turn out to be diagonally opposite to each other. Consequently, Bob's detectors do not register any clicks in such cases. Therefore, the efficiency of this attack, by design, is fundamentally limited to 50% on Bob's side. Here the proposed double-blinding attack involves a similar implementation to the single-blinding attack, but with the key difference that Eve blinds all detectors on both sides instead of just Bob's detectors. Due to the double-blinding attack, Alice and Bob are unable to detect the presence of Eve, resulting in a complete elimination of information leakage. In other words, the measure of information leakage, denoted as τ becomes zero in this scenario.

5.4 Keyrate for E91

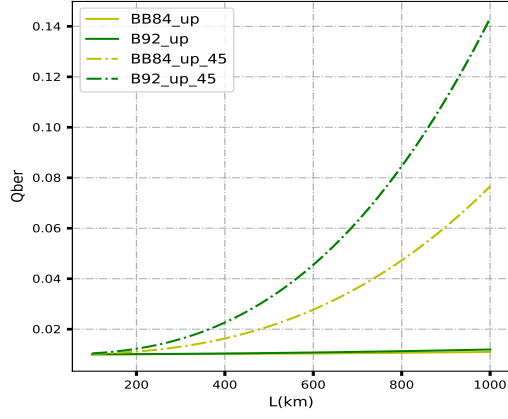
$$R_{E91} = \frac{p_{coin}}{3} \{ \tau(e_{91}) + f(e_{91})(e_{91} \log_2(e_{91}) + (1 - e_{91}) \log_2(1 - e_{91})) \}, \quad (57)$$

here $\frac{1}{3}$ is Sifting Factor because we use three basis in E91. The parameters used in Eq.(57) have been described above.

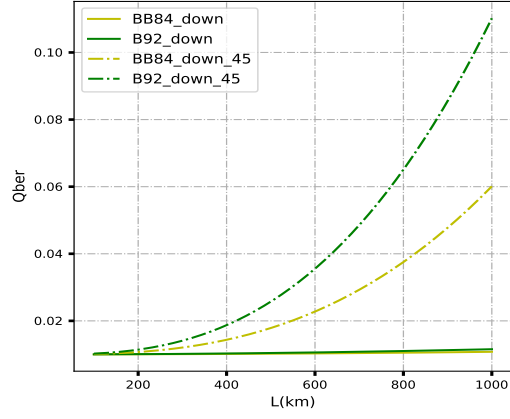
6 Numerical Results and Discussion

We have done a comparison between the BB84 and B92 Protocols for both the uplink and downlink communication scenarios. Our focus is to examine the relationship between channel length and two key metrics: the QBER and the keyrate. The simulated results, depicted in Fig.2 and Fig.3 showcase these dependencies under two different zenith angles: 0° and 45° , for both the uplink and downlink scenarios.

Further, we have done comparison for BBM92 and E91 protocols, which are entanglement-based protocols, for both the uplink and downlink scenarios at two distinct Zenith angles: 0° and 45° . The outcomes of this comparison are illustrated in Fig.4 and Fig.5 below.

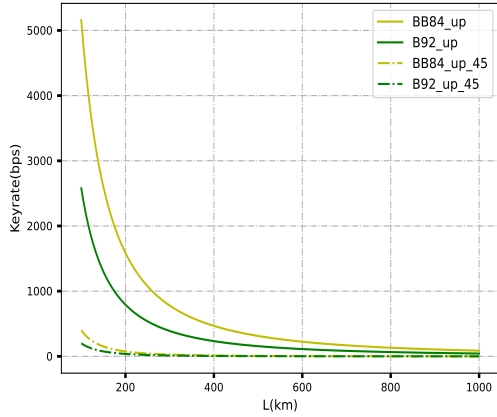


(a)

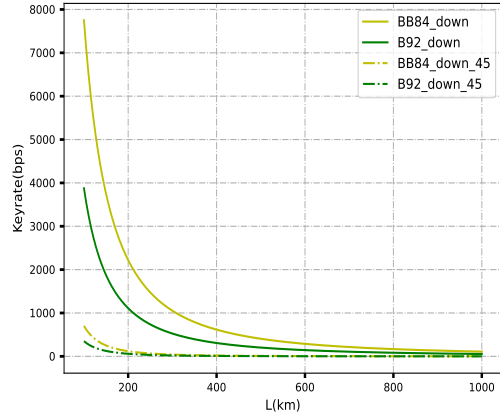


(b)

Figure 2: (a) Comparison of QBER for BB84 and B92 protocols with distance for uplink at 0° and 45° zenith angles, (b) Comparison of QBER for BB84 and B92 protocols with distance for downlink at 0° and 45° zenith angles. The bold curves represent 0° zenith angle and the dash curves represent 45° zenith angle.

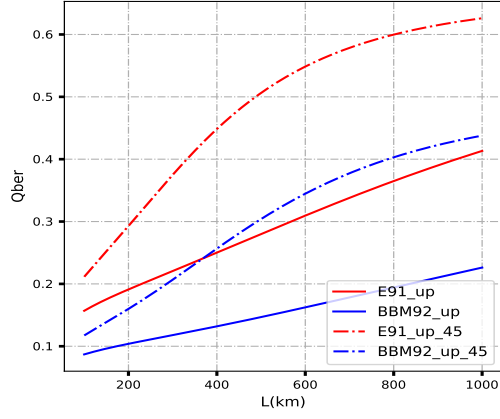


(a)

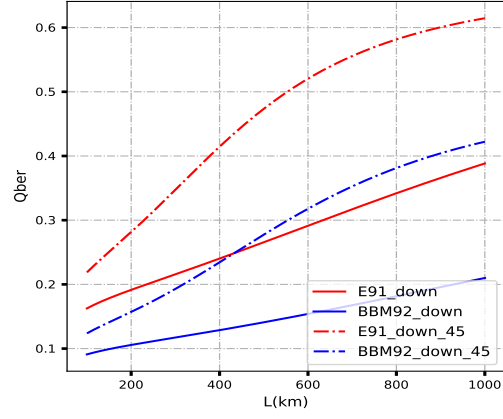


(b)

Figure 3: (a) Comparison of keyrate for BB84 and B92 protocols with distance for uplink at 0° and 45° zenith angles, (b) Comparison of keyrate for BB84 and B92 protocols with distance for downlink at 0° and 45° zenith angles. The bold curves represent 0° zenith angle and the dash curves represent 45° zenith angle.

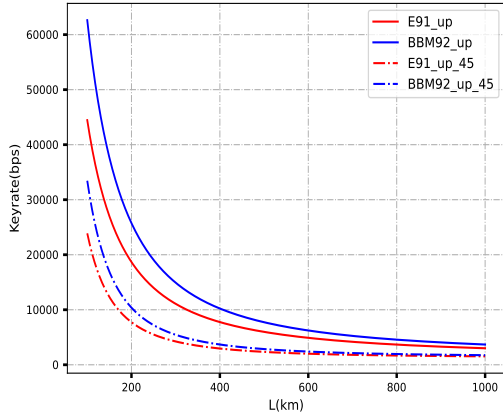


(a)

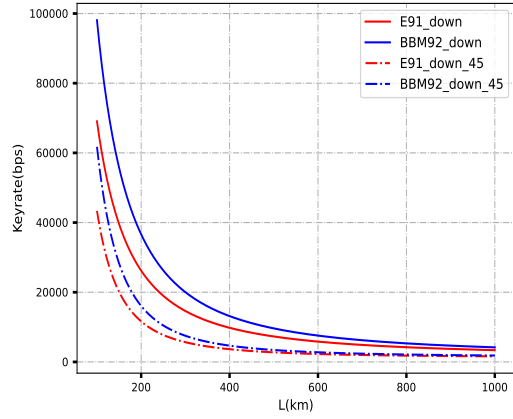


(b)

Figure 4: (a) Comparison of QBER for BBM92 and E91 protocols with distance for uplink at 0° and 45° zenith angles , (b) Comparison of QBER for BBM92 and E91 protocols with distance for downlink at 0° and 45° zenith angles. The bold curves represent 0° zenith angle and the dash curves represent 45° zenith angle.



(a)



(b)

Figure 5: (a) Comparison of keyrate for BBM92 and E91 protocols with distance for uplink at 0° and 45° zenith angles, (b) Comparison of keyrate for BBM92 and E91 protocols with distance for downlink at 0° and 45° zenith angles. The bold curves represent 0° zenith angle and the dash curves represent 45° zenith angle.

QBER Performance:

Based on the QBER expression for QKD link, we have done numerical simulations for laser links between a ground station and a satellite in low Earth orbit. Our simulations have been carried out at an operating wavelength of 800 nm, with an average photon number $\mu = 1$ for BB84 and B92 protocols and an ideal entangled photon source for BBM92 and E91 protocols. The plots shown in Fig.2 and Fig.4 demonstrates that the QBER tends to increase as the distance between the ground station and the satellite increases. The QBER exhibits a rising trend with increasing distance for both the uplink and downlink scenarios. Moreover, when comparing the uplink and downlink scenarios, it is evident that the QBER values are consistently higher in the uplink for all the aforementioned protocols.

As expected, the introduction of additional losses in the quantum channel leads to an increase in the QBER values. This relationship is clearly observed in the Fig.2 and Fig.4 by varying the communication distance. We have calculated QBER for 0° and 45° zenith angles and observed that the QBER is lower for the 0° zenith angle compared to the 45° zenith angle. This difference can be attributed to the shorter distance associated with the 0° zenith angle, as opposed to the longer distance at the 45° zenith angle. The reduced distance at 0° zenith angle result in lower losses and improved signal quality, leading to a lower QBER. By analyzing the obtained QBER values, it has been observed that the BB84 protocol exhibits greater stability against the channel losses compared to the B92 protocol. Similarly, comparison between BBM92 and E91 protocols reveals that E91 has more QBER than BBM92.

Keyrate Performance:

In Fig.3 and Fig.5, the keyrate is plotted as a function of distance. In our numerical analysis, different parameters are carefully considered, among which are the dark count rate of the detector set to 4×10^{-8} , the repetition rate of the laser source is 10MHz . Moreover, as previously stated, this repetition rate is chosen because it is the maximum achievable with existing APD detectors available. A comparison between BB84 and B92 protocols reveals that BB84 exhibits a higher key rate and hence more stable.

Fig.5(a) depicts the key generation rate as a function of distance for Ground-to-Satellite communication and Fig.5(b) shows the key generation rate as a function of distance for Satellite-to-Ground for BBM92 and E91 protocols. The obtained keyrate brings out that BBM92 protocol is more stable against channel loss as compared to E91 protocol.

7 Conclusion

We have compared the performance of the BB84 and B92 protocols as well as BBM92 and E91 Entangled based protocols for laser links between a ground station and a satellite in low Earth orbit. The QBER calculation was done using above mentioned losses for all four protocols. The expressions for the quantum keyrate were given for the ideal single photon sources for BBM92 and E91 protocols with some modifications. Similarly, the expressions for the quantum keyrate were given for the single photon sources for BB84 and B92 protocols with some modifications. On this basis, an evaluation of the quantum keyrate including various losses for the laser links between a ground station and a satellite for both uplink and downlink in the low earth orbit were performed at 0° and 45° zenith angles. It was observed that 0° zenith angle has more keyrate than 45° zenith angle in both uplink and downlink scenarios. This indicates that the shorter distance and associated reduced losses at the 0° zenith angle contribute to an increased key rate in the communication between the ground station and the satellite. Also the presented theoretical analysis results show that BB84 protocol can ensure the distribution of high secure keyrate for a given distance in comparison to the B92 and BBM92 ensures higher keyrate for a given distance in comparison to E91 protocol.

Acknowledgements

The author would like to thank CSIR for the fellowship support. SB acknowledges support from Interdisciplinary Cyber Physical Systems (ICPS) programme of the Department of Science and Technology (DST),

India, Grant No.:DST/ICPS/QuST/Theme-1/2019/6. SB also acknowledges the valuable contribution of the Defense Research and Development Organization (DRDO).

Declarations

The authors declare no conflicts of interest related to this research.

Data Availability Statement

Data sharing is not applicable to this article as no datasets were generated or analyzed during the current study.

References

- [1] Anirban Pathak. *Elements of quantum computation and quantum communication*. CRC Press Boca Raton, 2013, Chapter-8.
- [2] Arockia Bazil Raj, Vishal Sharma, and Subhashish Banerjee. Principle and applications of free space optical communication. *IET, UK*, 2019.
- [3] Dagmar Bruss, Gábor Erdélyi, Tim Meyer, Tobias Riege, and Jörg Rothe. Quantum cryptography: A survey. *ACM Computing Surveys (CSUR)*, 39(2):6–es, 2007.
- [4] S. Pirandola, U. L. Andersen, L. Banchi, M. Berta, D. Bunandar, R. Colbeck, D. Englund, T. Gehring, C. Lupo, C. Ottaviani, J. L. Pereira, M. Razavi, J. Shamsul Shaari, M. Tomamichel, V. C. Usenko, G. Vallone, P. Villoresi, and P. Wallden. Advances in quantum cryptography. *Advances in Optics and Photonics*, 12(4):1012, dec 2020.
- [5] Nicolas Gisin, Grégoire Ribordy, Wolfgang Tittel, and Hugo Zbinden. Quantum cryptography. *Rev. Mod. Phys.*, 74:145–195, 2002.
- [6] William K. Wootters and Wojciech H. Zurek. A single quantum cannot be cloned. *Nature*, 299:802–803, 1982.
- [7] N Srinatha, S Omkar, R Srikanth, Subhashish Banerjee, and Anirban Pathak. The quantum cryptographic switch. *Quantum information processing*, 13:59–70, 2014.
- [8] Charles H Bennett and Gilles Brassard. Quantum cryptography: Public key distribution and coin tossing. *arXiv preprint arXiv:2003.06557*, 2020.
- [9] Charles H. Bennett, François Bessette, Gilles Brassard, Louis Salvail, and John A. Smolin. Experimental quantum cryptography. *Journal of Cryptology*, 5:3–28, 1991.
- [10] W. T. Buttler, R. J. Hughes, P. G. Kwiat, S. K. Lamoreaux, G. G. Luther, G. L. Morgan, J. E. Nordholt, C. G. Peterson, and C. M. Simmons. Practical free-space quantum key distribution over 1 km. *Phys. Rev. Lett.*, 81:3283–3286, 1998.
- [11] Edo Waks, Assaf Zeevi, and Yoshihisa Yamamoto. Security of quantum key distribution with entangled photons against individual attacks. *Phys. Rev. A*, 65:052310, 2002.
- [12] Tobias Schmitt-Manderbach, Henning Weier, Martin Fürst, Rupert Ursin, Felix Tiefenbacher, Thomas Scheidl, Josep Perdigues, Zoran Sodnik, Christian Kurtsiefer, John G. Rarity, Anton Zeilinger, and Harald Weinfurter. Experimental demonstration of free-space decoy-state quantum key distribution over 144 km. *Phys. Rev. Lett.*, 98:010504, 2007.
- [13] Kishore Thapliyal, Anirban Pathak, and Subhashish Banerjee. Quantum cryptography over non-markovian channels. *Quantum Information Processing*, 16:1–21, 2017.
- [14] Vishal Sharma and Subhashish Banerjee. Analysis of atmospheric effects on satellite-based quantum communication: a comparative study. *Quantum Information Processing*, 18:1–24, 2019.

- [15] Theresa H Carbonneau and David Roger Wisely. Opportunities and challenges for optical wireless: the competitive advantage of free space telecommunications links in today's crowded marketplace. *Wireless Technologies and Systems: Millimeter-Wave and Optical*, 3232:119–128, 1998.
- [16] Charles H Bennett, François Bessette, Gilles Brassard, and Louis Salvail. J.Smolín, “Experimental quantum cryptography”. *J. Cryptol*, 5(1):3–28, 1992.
- [17] Hugo Zbinden, Nicolas Gisin, Bruno Huttner, Antoine Muller, and Wolfgang Tittel. Practical aspects of quantum cryptographic key distribution. *Journal of Cryptology*, 13:207–220, 2000.
- [18] PCM Owens, JG Rarity, PR Tapster, D Knight, and PD Townsend. Photon counting with passively quenched germanium avalanche. *Applied Optics*, 33(30):6895–6901, 1994.
- [19] Kevin J Resch, M Lindenthal, B Blauensteiner, HR Böhm, A Fedrizzi, C Kurtsiefer, A Poppe, T Schmitt-Manderbach, M Taraba, R Ursin, et al. Distributing entanglement and single photons through an intra-city, free-space quantum channel. *Optics Express*, 13(1):202–209, 2005.
- [20] Dominic Mayers. Unconditional security in quantum cryptography. *Journal of the ACM (JACM)*, 48(3):351–406, 2001.
- [21] Andrew Shields and Zhiliang Yuan. Key to the quantum industry. *Physics World*, 20(3):24, 2007.
- [22] Mehrdad S Sharbaf. Quantum cryptography: An emerging technology in network security. In *2011 IEEE International Conference on Technologies for Homeland Security (HST)*, pages 13–19. IEEE, 2011.
- [23] WT Buttler, RJ Hughes, Paul G Kwiat, SK Lamoreaux, GG Luther, GL Morgan, JE Nordholt, CG Peterson, and CM Simmons. Practical free-space quantum key distribution over 1 km. *Physical Review Letters*, 81(15):3283, 1998.
- [24] Christian Kurtsiefer, P Zarda, M Halder, Ph M Gorman, Paul R Tapster, JG Rarity, and Harald Weinfurter. Long-distance free-space quantum cryptography. In *Quantum Optics in Computing and Communications*, volume 4917, pages 25–31. SPIE, 2002.
- [25] Vishal Sharma, Chitra Shukla, Subhashish Banerjee, and Anirban Pathak. Controlled bidirectional remote state preparation in noisy environment: a generalized view. *Quantum Information Processing*, 14:3441–3464, 2015.
- [26] Jasmininder S Sidhu, Siddarth K Joshi, Mustafa Gündoğan, Thomas Brougham, David Lowndes, Luca Mazzarella, Markus Krutzik, Sonali Mohapatra, Daniele Dequal, Giuseppe Vallone, et al. Advances in space quantum communications. *IET Quantum Communication*, 2(4):182–217, 2021.
- [27] Sebastian Ecker, Bo Liu, Johannes Handsteiner, Matthias Fink, Dominik Rauch, Fabian Steinlechner, Thomas Scheidl, Anton Zeilinger, and Rupert Ursin. Strategies for achieving high key rates in satellite-based qkd. *npj Quantum Information*, 7(1):5, 2021.
- [28] Valentina Marulanda Acosta, Daniele Dequal, Matteo Schiavon, Aurélie Montmerle-Bonnefois, Caroline B Lim, Jean-Marc Conan, and Eleni Diamanti. Analysis of satellite-to-ground quantum key distribution with adaptive optics. *arXiv preprint arXiv:2111.06747*, 2021.
- [29] S. Kaur. Analysis of inter-satellite free-space optical link performance considering different system parameters. *Opto-Electronics Review*, 27(1):10–13, 2019.
- [30] Vishal Sharma. Effect of noise on practical quantum communication systems. *Defence Science Journal*, 66(2):186–192, 2016.
- [31] Robert Bedington, Juan Miguel Arrazola, and Alexander Ling. Progress in satellite quantum key distribution. *npj Quantum Information*, 3:1–30, 2017.
- [32] Vishal Sharma, U Shrikant, R Srikanth, and Subhashish Banerjee. Decoherence can help quantum cryptographic security. *Quantum Information Processing*, 17:1–16, 2018.
- [33] Vishal Sharma and Subhashish Banerjee. Analysis of quantum key distribution based satellite communication. In *2018 9th International Conference on Computing, Communication and Networking Technologies (ICCCNT)*, pages 1–5. IEEE, 2018.

- [34] Arindam Dutta and Anirban Pathak. Controlled secure direct quantum communication inspired scheme for quantum identity authentication. *Quantum Information Processing*, 22(13), 2022.
- [35] Arindam Dutta and Anirban Pathak. A short review on quantum identity authentication protocols: How would Bob know that he is talking with Alice? *Quantum Information Processing*, 21:369, 2022.
- [36] Richard J Hughes, Jane E Nordholt, Derek Derkacs, and Charles G Peterson. Practical free-space quantum key distribution over 10 km in daylight and at night. *New journal of physics*, 4(1):43, jul 2002.
- [37] Charles H. Bennett. Quantum cryptography using any two nonorthogonal states. *Phys. Rev. Lett.*, 68, 1992.
- [38] Artur K Ekert. Quantum cryptography based on bell’s theorem. *Physical review letters*, 67(6):661, 1991.
- [39] Marcos Curty, Maciej Lewenstein, and Norbert Lütkenhaus. Entanglement as a precondition for secure quantum key distribution. *Physical review letters*, 92(21):217903, 2004.
- [40] Charles H Bennett, Gilles Brassard, and N David Mermin. Quantum cryptography without bell’s theorem. *Physical review letters*, 68(5):557, 1992.
- [41] Abdulsalam G Alkholidi and Khalil S Altowij. Climate effects on performance of free space optical communication systems in yemen. *Frontiers of Optoelectronics*, 7:91–101, 2014.
- [42] Norhanis Aida M Nor, Md Rafiqul Islam, Wajdi Al-Khateeb, and AZ Suriza. Atmospheric effects on free space earth-to-satellite optical link in tropical climate. *International Journal of Computer Science, Engineering and Applications*, 3(1):17, 2013.
- [43] Samkelisiwe Purity Phehlukwayo, Marie Louise Umuhire, Yaseera Ismail, Stuti Joshi, and Francesco Petruccione. Influence of coincidence detection through free-space atmospheric turbulence using partial spatial coherence. *arXiv preprint arXiv:2006.12911*, 2020.
- [44] Hennes Henniger and Otakar Wilfert. An introduction to free-space optical communications. *Radio-engineering*, 19(2), 2010.
- [45] Dirk Giggenbach and Hennes Henniger. Errata: Fading-loss assessment in atmospheric free-space optical communication links with on-off keying. *Optical Engineering*, 47(6):069801, 2008.
- [46] Arun Majumdar. Free-space laser communication performance in the atmospheric channel. *Journal of Optical and Fiber Communications Reports*, 2:345–396, 2005.
- [47] Larry C Andrews and Ronald L Phillips. Laser beam propagation through random media. *Laser Beam Propagation Through Random Media: Second Edition*, 2005.
- [48] Larry C Andrews, Ronald L Phillips, Richard J Sasiela, and Ronald R Parenti. Strehl ratio and scintillation theory for uplink gaussian-beam waves: beam wander effects. *Optical Engineering*, 45(7):076001–076001, 2006.
- [49] Hong Guo, Bin Luo, Yongxiong Ren, Sinan Zhao, and Anhong Dang. Influence of beam wander on uplink of ground-to-satellite laser communication and optimization for transmitter beam radius. *Opt. Lett.*, 35(12):1977–1979, Jun 2010.
- [50] Nedasadat Hosseini-dehaj. *Continuous-Variable Quantum Communication over Free-Space Lossy Channels*. PhD thesis, UNSW Sydney, 2017.
- [51] Harjeevan Singh and Nitin Mittal. Link budget analysis of free space optical communication link for atmospheric conditions of india. *Materials Today: Proceedings*, 48:1064–1069, 2022.
- [52] Mohamed Alzenad, Muhammad Zeeshan Shakir, and Mohamed-Slim Alouini. Fso-based vertical backhaul/fronthaul framework for 5g+ wireless networks. *IEEE Communications Magazine*, 56, 12 2016.
- [53] Laszlo Bacsardi, Mate Galambos, Sandor Imre, and Andras Kiss. Quantum key distribution over space-space laser communication links. In *AIAA SPACE 2012 Conference & Exposition*, page 5265, 2012.

- [54] M.F. Abdul Khir, M.N. Mohd Zain, Iskandar Bahari, Suryadi, and S. Shaari. Implementation of two way quantum key distribution protocol with decoy state. *Optics Communications*, 285(5):842–845, 2012.
- [55] R. Etengu, F. M. Abbou, H. Y. Wong, A. Abid, N. Nortiza, and A. Setharaman. Performance comparison of BB84 and B92 satellite-based free space quantum optical communication systems in the presence of channel effects. *Journal of Optical Communications*, 32(1):37–47, 2011.
- [56] G. Adenier, Irina Basieva, Andrei Yu. Khrennikov, Masanori Ohya, and Noboru Watanabe. Double blinding-attack on entanglement-based quantum key distribution protocols. *Foundations of probability and physics*, 1424:9–16, 2011.